Article type : Special Issue Research Article

SPECIAL ISSUE RESEARCH ARTICLE

Kinetic Control in the Regioselective Alkylation of Pterin Sensitizers: A Synthetic, Photochemical, and Theoretical Study

Niluksha Walalawela[1,2], Mariana Vignoni[1,3], María Noel Urrutia[3], Sarah J. Belh[1,2], Edyta M. Greer[4*], Andrés H. Thomas[3*], and Alexander Greer[1,2*]

[1]Department of Chemistry, Brooklyn College, City University of New York, Brooklyn, New York 11210, United States

[2]Ph.D. Program in Chemistry, The Graduate Center of the City University of New York, 365 Fifth Avenue, New York, New York 10016, United States

[3]Instituto de Investigaciones Fisicoquímicas Teóricas y Aplicadas (INIFTA), Departamento de Química, Facultad de Ciencias Exactas, Universidad Nacional de La Plata (UNLP), CCT La Plata-CONICET, Casilla de Correo 16, Sucursal 4, (1900) La Plata, Argentina

[4] Department of Natural Sciences, Baruch College, City University of New York, New York, NY 10010, United States

*Corresponding authors' email addresses: athomas@inifta.unlp.edu.ar (Andrés H. Thomas); edyta.greer@baruch.cuny.edu (Edyta M. Greer); and agreer@brooklyn.cuny.edu (Alexander Greer)

ABSTRACT

Alkylation patterns and excited state properties of pterins were examined both experimentally and theoretically. 2D NMR spectroscopy was used to characterize the pterin derivatives, revealing undoubtedly that the decyl chains were coupled to either the O4 or N3 sites on the pterin. At a temperature of 70 °C the pterin alkylation regioselectively favored the O4 over the N3. The O4 was also favored when using solvents in which the reactants had increased solubility, namely *N,N*-dimethylformamide and *N,N*-dimethylacetamide, rather than solvents in which the reactants had very low solubility (tetrahydrofuran and dichloromethane). Density functional theory (DFT) computed enthalpies correlate to regioselectivity being kinetically driven because the less stable *O*-isomer forms in higher yield than the more stable *N*-isomer. Once formed these compounds did not interconvert thermally or undergo a unimolecular "walk" rearrangement. Mechanistic rationale for the factors underlying the regioselective alkylation of pterins is suggested, where kinetic rather than thermodynamic factors are key in the higher yield of the *O*-isomer. Computations also predicted greater solubility and reduced triplet state energetics thereby improving the properties of the alkylated pterins as $^1O_2$ sensitizers. Insight on thermal and photostability of the alkylated pterins is also provided.

INTRODUCTION

Despite their low solubility in every solvent, a number of studies have been done on the photochemistry of pterin sensitizers (1-5). A *N*-methyl pterin **2** (6) as well as other pterin derivatives (7) have been previously reported. We recently reported on alkyl substituted pterins **3** and **4** which, due to the alkyl group [$CH_3(CH_2)_9$], were soluble in organic solvents (Figure 1) (8).

Similarly, organic chemists doing mechanistic studies will often use substituents to make otherwise insoluble molecules solvate. For instance, *t*-butyldimethylsilyl substituents have been connected to the sugar of guanosine **6** in order to have the guanosine solvate (9-12). Various

sensitizers such as porphyrins and chlorins have also had alkyl substituents or PEG substituents attached in order to enhance their solubility (13-16). Conjugated polymers with a ratiometric fluorescent response to singlet oxygen have also been solubilized with ethyl and hexyl substituents (17). There are other uses for alkyl-substituted sensitizers, e.g., **5** (18), such as membrane binding (19-25), but little information exists in this vein for pterins.

Our preliminary synthetic and photochemical work with alkylated pterins **3** and **4** (8) was a first step. Substituted pterins had been previously reported. However, regioselectivity is yet to be achieved in nucleophilic substitutions with pterins. In contrast, regioselectivity has been achieved in nucleophilic substitutions with other sensitizers, such as porphyrins (26).

We hypothesized that both kinetic and thermodynamic principles would determine the stability of *O*- vs *N*-alkylated pterins. We also thought that alkylation of pterins would enable better control of their solubility and excited state properties. In order to test these ideas, we examined pterins with methyl and decyl substitutions on the *O*- and *N*-sites of the amide group (Figure 1). We aimed to determine: (1) whether pterins with decyl chain substituents could be further characterized by 2D NMR spectroscopy, (2) whether regioselectivity in the alkylation depends on temperature, solvent, or base, (3) whether computed enthalpies were related to the regioselectivity, and whether the attached alkyl group migrates around the pterin periphery via a "walk rearrangement", (4) whether computed solubilities predict lipophilic amplification in pterins **3** and **4** compared to pterins **1** and **2**, (5) whether pterin alkylation perturbs the excited state energies and photostability, and (6) how the mechanism can be summarized. The results obtained here point to kinetics, not thermodynamics, in the regioselective formation of alkyl pterin derivatives, including properties that improve pterins as sensitizers for type II ($^1O_2$) photosensitized oxidation reactions.

<Figure 1>

MATERIALS AND METHODS

Materials. Pterin **1**, 1-iododecane, sodium hydroxide (NaOH), potassium carbonate (K_2CO_3), hydrochloric acid (HCl), pyridine, *N,N*-dimethylformamide (DMF), *N,N*-dimethylacetamide (DMA), tetrahydrofuran (THF), dichloromethane (DCM), dimethylsulfoxide (DMSO), and DMSO-d_6, were obtained from Sigma and were used as received. Methanol and acetonitrile were from J. T. Baker (HPLC grade). Water was purified on a deionization system.

For the purification of compounds, flash chromatography was used with silica of a 200-400 particle size.

Equipment. Nuclear magnetic resonance (NMR) spectra were recorded on a Bruker instrument at 400 MHz for ^{1}H NMR and 100.6 MHz for ^{13}C NMR. High-performance liquid chromatography (HPLC) was carried out with a Prominence system from Shimadzu (solvent delivery module LC-20AT, on-line degasser DGU-20A5, communications bus module CBM-20, auto sampler SIL-20A HT, column oven CTO-10AS VP, photodiode array (PDA) detector SPD-M20A and fluorescence (FL) detector RF-20A) for monitoring of the photochemical reactions. A Synergi Polar-RP column (ether-linked phenyl phase with polar endcapping, 150 × 4.6 mm, 4 mm, Phenomenex) was used for product separation, with a flow of 0.3 mL/min and 90% of methanol and 10% of water were used as mobile phase.

Synthetic procedure. Pterins **3** and **4** were synthesized by a previously described method (8) with some modifications. Here, bases (NaOH or K_2CO_3) and solvents (DMF, THF, and DMA) were explored to expand on the previously studied conditions of K_2CO_3 in DMF (8). All reactions were performed under Ar and in anhydrous solvents. Base (NaOH or K_2CO_3, 1 equiv) was added to a solution of pterin **1** (1 equiv, 0.05-0.15 mmol) in anhydrous solvent (DMF, THF, or DMA, 10-12 mL). The mixture was sonicated and sparged with Ar for 20 min. Then, 1-iododecane (2 equiv) was added to the solution. The reaction mixture was placed into a water bath and was heated at 70 °C with stirring for 20 h. The solution was cooled to room temperature and the solvent was evaporated to dryness under vacuum. The solid products were treated with NaCl (s.s.) (10 mL) then extracted with DCM (3 × 10 mL). The organic layers were separated, dried over Na_2SO_4, filtrated and the solvent was evaporated to dryness. The white solid residue obtained was separated by silica gel column chromatography (eluent: DCM 100% followed by DCM-methanol up to 10% methanol).

<Figure 2>

*4-(Decyloxy)pteridin-2-amine (**3**).* ^{1}H NMR (400 MHz, DMSO-d_6) δ 8.78 (d, J = 2 Hz, 1H), 8.43 (d, J = 2 Hz, 1H), 7.28 (s, 2H), 4.46 (t, J = 7 Hz, 2H), 1.81 (m, 2H), 1.23 (m, 14H), 0.84 (t, J = 7 Hz, 3H) ppm. ^{13}C NMR (100.6 MHz, DMSO-d_6) δ 166.9, 161.6, 157.2, 150.9, 139.5, 123.4, 67.2, 31.3, 29.0, 28.9, 28.7, 28.6, 28.1, 25.4, 22.1, 14.0 ppm.

*2-Amino-3-decylpteridin-4(3H)-one (**4**).* ^{1}H NMR (400 MHz, DMSO-d_6) δ 8.66 (d, J = 2 Hz, 1H), 8.36 (d, J = 2 Hz, 1H), 7.59 (s, 2H), 3.95 (t, J = 7 Hz, 2H), 1.56 (m, 2H), 1.23 (m, 14H),

0.85 (t, J = 7 Hz, 3H) ppm. ^{13}C NMR (100.6 MHz, DMSO-d_6) δ 160.7, 155.8, 153.9, 150.0, 139.1, 128.0, 41.7, 26.8, 31.3, 28.9, 28.8, 28.7, 26.0, 22.1, 14.0 ppm.

Steady-State Photolysis. Continuous photolyses were carried out by irradiating samples in quartz cells (0.4 cm optical path length). Two Rayonet RPR 3500 lamps (Southern N.E. Ultraviolet Co.) with emission centered at 350 nm [band width (fwhm) 20 nm] were employed as radiation source. Photolysis experiments were performed in air-equilibrated aqueous dispersions. Using aberchrome 540 (Aberchromics, Ltd.) as an actinometer, the quantum yields of pterin disappearance (Φ) was determined using the following equation:

$$\Phi = - (d[compound]/dt)_0 / q^{0,V}_{n,p}$$

where $(d[compound]/dt)_0$ is the initial rate of compound consumption and $q^{0,V}_{n,p}$ is the incident photon flux density, which was found to be 2.5 (±0.2) × 10^{-5} Einstein L^{-1} s^{-1} at the excitation wavelength (27).

Computations. Density functional theory (DFT) calculations were carried out with the Gaussian 09 program package (28) and molecular structures were viewed with Gaussview 5 (29). The DFT functional used was B3LYP along with the D95** basis set (30). Frequency calculations established the type of stationary point obtained. Intrinsic reaction coordinate calculations demonstrated that saddle points connected minima. Thermal corrections for enthalpy were added at 298.15 K and 1 atm. Log *P* and log *D* values were computed with Marvin Sketch version 17.1.2 (ChemAxon Ltd. Budapest, Hungary) (31). For pterins **3** and **4**, the decyl group was optimized in a zigzag orientation of carbon atoms, i.e., an all *anti* conformation. To facilitate the convergence of the pterin **3** and **4** geometries, an extra quadratic convergence for self-consistent field method (scf = xqc) and an ultrafine integral (int = grid = ultrafine) were used. Time-dependent density functional theory (TD-DFT) calculations of vertically excited singlet (S_1) and triplet states (T_1) were carried out with B3LYP/D95** using the optimized singlet ground state (S_0) structures. B3LYP/D95** has been shown to perform well in predicting the excited state geometries and energetics of a series of heterocyclic and aromatic compounds (32).

RESULTS AND DISCUSSION

We present the results of a study of alkylated pterin sensitizers. First, we describe the synthesis and characterization of pterins **3** and **4**. Second, we examine the properties of alkyl pterins, including their excited-state energetics and photostability.

Synthesis and further characterization of pterins 3 and 4

Previously, we showed that the O4 and N3 of pterin **1** were the nucleophilic sites for alkylation with iododecane (8). In this study, we have collected 2D NMR spectra (HSQC and HMBC NMR) to complement the previously reported 1D NMR spectra (^{1}H and ^{13}C) (8) and provide additional spectroscopic evidence for pterin **3** and **4**. The carbon signals for **3** and **4** were definitively assigned through analysis of the ^{13}C, HSQC and HMBC NMR spectra (Tables 1-3, and Figures S1-S4, Supporting Information). Although, the key to the unambiguous assignment of the *O*- and *N*-alkylation were the HMBC NMR spectra.

Figure 3a is an expanded portion of HMBC spectrum for pterin **3** which shows the O−CH_2 protons (4.46 ppm) in relation with the aromatic carbons. Only one cross peak is observed suggesting an exocyclic connection for the alkyl chain, and ruling out an endocyclic connection, limiting the alkyl chain's location to O4 or N2. Furthermore, cross peak X shows a connection between the O−CH_2 (4.46 ppm) and carbon b, which is consistent with O4 alkylation. Acidic and basic conditions do not change the UV spectra of the pterin **3** further supporting the O4 alkylation assignment. Figure 3b is an expanded portion of the HMBC spectrum for pterin **4**, in which two observable cross peaks (Y,Z) suggest the alkyl chain is connected to an endocyclic nitrogen. The N−CH_2 peak (3.95 ppm) does not show any correlation with the e′, f′, c′ or d′ carbons ruling out alkylation at N1, N5 and N8. However, the N−CH_2 peak does show correlation with the a′ and b′ carbons suggesting alkylation at N3.

<Tables 1-3>

<Figure 3>

Temperature, solvent, and base dependence yields of pterins 3 and 4

Table 4 shows the percent yields of pterin **3** and **4** in reactions of pterin **1** carried out in the presence of K_2CO_3 in DMF at temperatures ranging from 25 °C to 90 °C. This study expands on the previously reported conditions of K_2CO_3 in DMF at 70 °C (8). We observe that there was no reaction at 25 °C up to 40 ^{o}C (entry 1). The reaction yielded products **3** and **4** at 60 ^{o}C in a 1.4:1

ratio, and a ratio of 1.85:1 at 70 ^{o}C (which was the optimum temperature for regioselectivity for obtaining pterin **3**) (entries 2 and 3). However, at 90 °C, there was no observed formation of products **3** and **4**, which is due to DMF condensation onto N2 site (entry 4).

Table 4 also shows the percent yields of pterin **3** and **4** in reactions of pterin **1** carried out in the presence of bases (K_2CO_3 or NaOH) in various solvents (DMF, DMA, THF, and DCM). We tested NaOH and found that no products were obtained in DMF (entry 5). The reaction in DMA was found to produce regioselectivity of 1.6:1 for **3**:**4** which was the highest seen in our solvent series. Reactions in THF and DCM led to pterins **3** and **4** at very low yields (entries 7 and 8). Reactions in THF give yields less than 10% with pterins **3** and **4** as the only products, which appears to be due to the low solubility of pterin **1** in these solvents. At present, we have not examined H-bonding solvents such as methanol to probe effects on the regioselectivity due to their nucleophilic reactivity with 1-iododecane. Even DMSO proved to be impractical in the synthesis due to low pterin solubility.

<Table 4>

Next, we wanted to investigate the stability of alkyl pterins, namely to see the relative energies of pterin isomers and determine whether pterins function as carriers of alkyl groups. Thus, we investigated this possibility with DFT.

DFT computed stabilities of alkyl pterin regioisomers

DFT computations provide a means of predicting the relative stability of isomeric alkylated pterins and possible mechanisms for the rearrangement of alkyl pterin. Calculations were performed on a methyl pterin derivative in order to understand the decyl group's impact on the "walk" rearrangement energetics (Figure 4). In Figure 5, three mechanisms can be envisioned for alkyl pterin rearrangement (neutral and anionic surfaces): (a) a concerted unimolecular through a alkyl "walk" rearrangement, (b) a dissociative pathway through an alkyl carbocation and pterin oxy anion formation, and (c) a dissociative pathway involving radical pair formation. We focused first on the concerted route (path A).

<Figures 4 and 5>

Figure 6A shows the relative enthalpies which were calculated for path A. The relative enthalpies for the *O*- and *N*-methyl pterins is 6.8 kcal/mol (**2b** and **2**, respectively), and for the *O*- and *N*-decyl pterins is 5.6 kcal/mol (**3** and **4**, respectively). In both cases the *N*-alkylated pterin is

computed to be more stable than the *O*-alkylated pterin. The relative enthalpies for anionic *O*- and *N*-methyl pterins were also carried out.

Figure 6B shows the calculated anionic surface, in which the *N*- and *O*-methyl pterin anions have a more pronounced stability difference of 23.1 kcal/mol than their neutral counterparts, with the *N*-methyl pterin remaining the more stable. The DFT calculations predict high activation enthalpies of 53.2 kcal/mol for the *O*- to *N*-rearrangement of methyl pterin through a concerted pathway. Further calculations on **2** and **2b** show that the formation of ion pair intermediates (path B) or radical pair (path C) both require greater than 60-kcal/mol of energy. The energy requirement for Path B is very high due to charge separation in the gas phase.

<Figure 6>

Figure 7 shows a computed energy diagram for a "walk" rearrangement of the methyl group around the periphery of the pterin ring in a counter clockwise direction. Relative enthalpies in kcal/mol of the pterin isomers and transition states are shown. The [1,3]- and [1,4]-methyl shifts require very high activation energies. Thus, it is logical to conclude that the *O*- and *N*-alkyl pterins, e.g., **3** and **4**, are non-interconverting species, unlike walk processes observed for molecular rearrangements (33-43), such as the walk rearrangement of bicyclo[2.1.0]pent-2-ene (44).

<Figure 7>

Computed solubilities

Table 5 lists the computed log *P* and log *D* values that were obtained with the ChemAxon algorithm. Computationally, we have found that the more lipophilic decylated pterins **3** and **4** show a three to four fold increase in their computed solubilities as compared to the parent pterin **1**. Experimentally, we have found this increase in solubility to be true for organic solvents. Similarly, the computed log *D* values are higher for the decylated pterins **3** and **4** than the methyl pterin **2** or parent pterin **1**. The computed log *D* results with parent pterin **1** are in-line with literature, sparing solubility in water and very low solubility in most organic solvents (8,45-47). As shown in literature, covalently attaching an alkane chain, e.g. from a $-CH_2-$ to $-(CH_2)_8-$

bridging, to a dye, e.g. diketo-pyrrolo-pyrrole dye, increases the dye's solubility in organic solvents (48). One reference showed that the increase in solubility could be as high as by a factor of 60 (49). Computations were used not only to predict alkyl pterin lipophilicity, but also excited state energetics.

<Table 5>

Computed excited state energies and photostability

Next, theoretical calculations were carried out to examine whether the alkylation of pterins perturbs their excited state energetics and photostability. Table 6 shows the computed vertical transition energies ($S_0 - S_1$ and $S_0 - T_1$) upon alkylation of pterin with methyl or decyl groups. The computed results show the proper ordering of the pterin excited states. However, these calculations overestimate the singlet and triplet transition energies by ~10 kcal/mol, whether solvent is accounted for or not in the calculation. Time-dependent DFT enabled the computation of the triplet energies, and yield some insight about their potential as triplet sensitizers for the formation of $^1O_2$. Singlet oxygen forms mainly via energy transfer from the T_1 state of the sensitizer. That is, alkylation of pterin led to lower triplet energies, which is consistent with the previously reported enhanced $^1O_2$ quantum yield data (8). Pterin **1** has the highest-lying computed triplet (T_1 = 68.0 kcal/mol) of the series. Pterin alkylation at either O4 or N3 lowers T_1 by 0.4-3.6 kcal/mol compared to parent pterin **1**. An analysis between pterins **3** and **4** reveal further differences. Alkylation at O4 leads to a stabilizing effect and lowers the excited state energies compared to alkylation at N3. That is, *O*-alkylated pterin **3** has a $S_0 - S_1$ transition of ~76 kcal/mol and a $S_0 - T_1$ transition of ~64 kcal/mol. In contrast, *N*-alkylated pterin **4** has a higher $S_0 - S_1$ transition of ~81 kcal/mol and a higher $S_0 - T_1$ transition of ~68 kcal/mol.

<Table 6>

Table 7 and Figure 8 show further computed data on electronic excitations of parent pterin **1** and alkylated pterins **2-4**. We observe an intense $S_0 - T_1$ transition for pterins **1**, **2**, and **4** is the HOMO-1 $\rightarrow$ LUMO transition. The HOMO-1 possesses nonbonding character with involvement of the σ-bonding orbitals from the alkyl group, while the LUMO possesses π-antibonding character. Thus, the $S_0 - T_1$ transition for pterins **1**, **2**, and **4** is described as n $\rightarrow$ π* transition. On the other hand, the most intense $S_0 - T_1$ transition for pterins **2b** and **3** is the

HOMO → LUMO transition, where the HOMO has π-bonding character, and the LUMO has π-antibonding character. Thus, $S_0 - T_1$ transition for pterins **2b** and **3** can be described as π → π* transition. The above results are consistent with literature (50), which had focused more on singlet excited state properties than we do here. Notably in Figure 8, the alkylated pterins show contributions of σ orbitals from alkyl of methyl or decyl groups to HOMO-1, HOMO, and LUMO orbitals and appear to provide stability compared to parent pterin **1**. Given the above computed information, we wanted to assess whether pterin alkylation increased photostability, as we discuss next.

<Table 7>

<Figure 8>

In terms of photostability, our previous report (8) showed that the decyl chain pterins **3** and **4** degrade under UVA illumination. In the current paper, we expand on this topic where Figure 9 shows an HPLC trace of pterin **3** (retention time = 13.8 min) that decomposes upon UVA irradiation. While several photodegradation products appear with retention times ranging from 6-11 min, they have not been characterized. The inset shows a decrease of the concentration as a function of time, where the corresponding quantum yield of consumption (Φ_{consum}) pterin **3** was found to be 4.3 (±0.7) × 10^{-4}, which is slightly lower than the Φ_{consum} for pterin **1** (8.2 × 10^{-4}) and for pterin **1** anion (1.2 × 10^{-3}) (5). We believe that the photodegradation process is indicative of sensitizers bearing free amine groups, which are thus prone to type I photosensitized oxidation reactions (electron transfer and H atom abstraction) and decomposition (51-53). Relatedly, there are reports of pterins that upon irradiation form radicals (54,55), including radicals from the $^3\pi\pi^*$ state in the presence of O_2 (56).

<Figure 9>

Mechanistic summary

Here, we postulate on pterin alkylation patterns, and thermal and photostability. Our 2D NMR data provided evidence that the decyl group attaches to pterin at the O4 or N3 position. There was no evidence for alkylation at any other position. The nucleophilicity at O4 and N3 are similar, this is apparent due to the ~1.6:1 ratios of both isomers. Solvents DMF and DMA are superior to THF and DCM as the reactant pterin **1** is more highly soluble in the former two

solvents. One reason the solubility enhancement is so beneficial is that the reactions of pterins are not amenable to common organic solvents and purification techniques. In addition to solubility enhancements, it is logical to suggest an increase in the pterins' resistance against forming of aggregates due to alkylation, similar instances of deaggregation of porphyrins and other aromatics due to alkylation in organic solvents (57-65). This decrease in aggregation has proven necessary to improve sensitizer performance (66-68). Both the computational and experimental work indicates that alkyl substitution in pterins lower the triplet energies and improve their performance as $^1O_2$ sensitizers. Indeed, the photostability increases slightly upon alkylation of pterin, which is also beneficial. Apart from solubility and stability issues, the alkylation enables pterins **3** and **4** to serve as sensitizers within membrane locales, halting pterins' tendency to traverse across membranes.

CONCLUSION

In this paper we report on our study of the regioselective alkylation and excited state properties of pterins. Our study has provided evidence for kinetics and nucleophilicity being the dominate factors, rather than thermodynamics and basicity in determining the regioselectivity of these reactions. This gives us insight into controlling the selective formation of pterin derivatives. One further benefit to our success in the regioselective alkylation of pterin is the potential to attach other substituents, such as $CH_2CH_2CF_2CF_2CF_2CF_3$, to solubilize pterins in fluorous phases for a possible amplification of type II at the expense of type I at fluorous solvent-water interfaces.

ACKNOWLEDGEMENTS. N.W., S.J.B. and A.G. acknowledge support from the NSF (CHE-1464975). N.W acknowledges support from a Rose K. Rose Dissertation Award and a Graduate Center Doctoral Student Research Grant (DSRG 12). We acknowledge support from Consejo Nacional de Investigaciones Científicas y Técnicas (CONICET) and the National Science Foundation (NSF) through the Bilateral Cooperation Programme, Level I (PCB-I, Res.2172). M.V., M.N.U. and A.H.T. acknowledge support from CONICET (Grant PIP 0304), Agencia de Promoción Científica y Tecnológica (ANPCyT-Grant PICT 2012-0508 and 2015-1988) and Universidad Nacional de La Plata (UNLP-Grant X712). E.M.G. acknowledges support from the

donors of the Petroleum Research Fund of the American Chemical Society. Computational support was provided by the Extreme Science and Engineering Discovery Environment (XSEDE), which is supported by the National Science Foundation Grant No. ACI01053575. A.G. acknowledges support from the Leonard and Claire Tow Professorship at Brooklyn College. M.V. thanks the Programa de Financiamiento de Estadías en el Exterior from CONICET. M. N. U. thanks CONICET for postdoctoral research fellowship. M.V. and A.H.T. are research members of CONICET. We thank Leda Lee for the graphic arts work.

SUPPORTING INFORMATION

Additional Supporting Information is available in the online version of this article:

Figure S1. HSQC NMR spectra of pterin **3** in DMSO-d_6.

Figure S2. HMBC NMR spectra of pterin **3** in DMSO-d_6.

Figure S3. HSQC NMR spectra of pterin **4** DMSO-d_6.

Figure S4. HMBC NMR spectra of pterin **4** DMSO-d_6.

REFERENCES

(1) Serrano, M. P., S. Estébanez, M. Vignoni, C. Lorente, P. Vicendo, E. Oliveros and A. H. Thomas (2017) Photosensitized Oxidation of 2′-Deoxyguanosine 5′-Monophosphate: Mechanism of the Competitive Reactions and Product Characterization. *New J. Chem.* **41**, 7273−7282.

(2) Serrano, M. P., M. Vignoni, C. Lorente, P. Vicendo, E. Oliveros and A. H. Thomas (2016) Thymidine Radical Formation via One-electron Transfer Oxidation Photoinduced by Pterin: Mechanism and Products Characterization. *Free Radic. Biol. Med.* **96**, 418–431.

(3) Reid, L. O., E. A. Roman, A. H. Thomas and M. L. Dántola (2016) Photooxidation of Tryptophan and Tyrosine Residues in Human Serum Albumin Sensitized by Pterin: A Model for Globular Protein Photodamage in Skin. *Biochemistry* **55**, 4777−4786.

(4) Thomas, A. H., Á. Catala and M. Vignoni (2016) Soybean Phosphatidylcholine Liposomes as Model Membranes to Study Lipid Peroxidation Photoinduced by Pterin. *Biochim. Biophys. Acta, Biomembr.* **1858**, 139−145.

(5) Lorente, C. and A. H. Thomas (2006) Photophysics and Photochemistry of Pterins in Aqueous Solution. *Acc. Chem. Res.* **39**, 395–402.

(6) Yao, Q. and W. Pfleiderer (2003) Pteridines. Part CXIII. *Helv. Chim. Acta.* **86**, 1-12.

(7) Glazer, E. C., Y. H. Le Nguyen, H. B. Gray and D. B. Goodin (2008) Probing Inducible Nitric Oxide Synthase with a Pterin-ruthenium(II) Sensitizer Wire. *Angew. Chem. Int. Ed.* **47**, 898-901.

(8) Vignoni, M., N. Walalawela, S. M. Bonesi, A. Greer and A. H. Thomas (2017) Lipophilic Decyl Chain-Pterin Conjugates with Sensitizer Properties. *Mol. Pharm.* Ahead of Print.

(9) Sheu, C. and C. S. Foote (1993) Endoperoxide Formation in a Guanosine Derivative. *J. Am. Chem. Soc.* **115**, 10446–10447.

(10) Sheu, C. and C. S. Foote (1995) Reactivity toward Singlet Oxygen of a 7,8-Dihydro-8-oxoguanosine ("8 Hydroxyguanosine") Formed by Photooxidation of a Guanosine Derivative. *J. Am. Chem. Soc.* **117**, 6439–6442.

(11) Sheu, C., P. Kang, S. Khan and C. S. Foote (2002) Low-Temperature Photosensitized Oxidation of a Guanosine Derivative and Formation of an Imidazole Ring-Opened Product. *J. Am. Chem. Soc.* **124**, 3905–3913.

(12) Kang, P. and C. S. Foote (2002) Formation of Transient Intermediates in Low-Temperature Photosensitized Oxidation of an 8-^{13}C-Guanosine Derivative. *J. Am. Chem. Soc.* **124**, 4865–4873.

(13) Schall, A. P., P. Iavicoli, Z.J. Qi, J. Menko, Y. Lu, M. Linares, J. C. de Paula, D.B. Amabilino, A.T. Johnson and W. F. Smith (2015) Photoconductivity of Nanofilaments That are Self-Assembled from a Porphyrin with Long Alkyl-Chain Substituents. *J. Phys. Chem. C.* **119**, 26154–26163.

(14) Battogtokh, G., H. Liu, S. Bae, P. K. Chaturvedi, Y. Kim, I. Kim and W. S. Ahn (2012) Synthesis of Chlorin-based Unsaturated Fatty Acid Conjugates: Their In Vitro Phototoxicity on TC-1 Cancer Cell Line. *J. Photochem. Photobiol. B: Biology* **110**, 50–57.

(15) Sholto, A. and B. Ehrenberg (2008) Hydrophobicity, Topography in Membranes and Photosensitization of Silicon Phthalocyanines with Axial Ligands of Varying Lengths. *Photochem. Photobiol. Sci.* **7**, 344–351.

(16) Kimani, S., G. Ghosh, A. A. Ghogare, B. Rudshteyn, D. Bartusik, T. Hasan and A. Greer (2012) Synthesis and Characterization of Mono-, Di-, and Tri-Poly(ethylene glycol) Chlorin e_6 Conjugates for the Photokilling of Human Ovarian Cancer Cells. *J. Org. Chem.* **77**, 10638–10647.

(17) Altinok, E., Z. C. Smith, Z. C and S. W. Thomas, III (2015) Two-Dimensional, Acene-Containing Conjugated Polymers That Show Ratiometric Fluorescent Response To Singlet Oxygen. *Macromolecules* **2015**, *48*, 6825–6831.

(18) Jadhav, S., C. Yim, J. Rajander, T. J. Gronroos, O. Solin and P. Virta (2016) Solid-Supported Porphyrins Useful for the Synthesis of Conjugates with Oligomeric Biomolecules. *Bioconjugate Chem.* **27**, 1023–1029.

(19) Timor, R., H. Weitman, N. Waiskopf, U. Banin and B. Ehrenberg (2015) PEG-Phospholipids Coated Quantum Rods as Amplifiers of the Photosensitization Process by FRET. *ACS Appl. Mater. Interfaces.* **7**, 21107–21114.

(20) Lavi, A., H. Weitman, R. T. Holmes, K. M. Smith and B. Ehrenberg (2002) The Depth of Porphyrin in a Membrane and the Membrane's Physical Properties Affect the Photosensitizing Efficiency. *Biophys. J.* **82**, 2101–2110.

(21) Bronshtein , I., K. M. Smith and B. Ehrenberg (2005) The Effect of pH on the Topography of Porphyrins in Lipid Membranes. *Photochem. Photobiol.* **81**, 446–51.

(22) Minnes, R., H. Weitman, Y. You, M. R. Detty and B. Ehrenberg (2008) Dithiaporphyrin Derivatives as Photosensitizers in Membranes and Cells. *J. Phys. Chem. B* **112**, 3268–3276.

(23) Sholto, A., S. Lee, B. M. Hoffman, A. G. M. Barrett and B. Ehrenberg (2008) Spectroscopy, Binding to Liposomes and Production of Singlet Oxygen by Porphyrazines with Modularly Variable Water Solubility. *J. Photochem. Photobiol.* **84**, 764–773.

(24) Nakagaki, M., H. Komatsu and T. Handa (1986) Effects of Lysophosphatidylcholine Micelle and Phosphatidylcholine Liposome on Photoreduction of Methylviologen. *Arch. Biochem. Biophys.* **249**, 388–396.

(25) Freitas, A. A., F. H. Quina, A. C. Fernandes and A. A. L. Maçanita (2010) Picosecond Dynamics of the Prototropic Reactions of 7-Hydroxyflavylium Photoacids Anchored at an Anionic Micellar Surface. *J. Phys. Chem. A.* **114**, 4188–4196.

(26) Senge, M. O. (2005) Nucleophilic Substitution as a Tool for the Synthesis of Unsymmetrical Porphyrins. *Acc. Chem. Res.* **38**, 733–743.

(27) Kuhn, H. J., S. E. Braslavsky and R. Schmidt (2004) Chemical Actinometry (IUPAC Technical Report). *Pure Appl. Chem.* **76**, 2105–2146.

(28) Gaussian 09, Revision D.01, M. J. Frisch, G. W. T. H. B. Schlegel, G. E. Scuseria, M. A. Robb, J. R. C. G. Scalmani, V. Barone, B. Mennucci, G. A. Petersson, H. N. M. Caricato, X. Li, H. P. Hratchian, A. F. Izmaylov, J. B. G. Zheng, J. L. Sonnenberg, M. Hada, M. Ehara, K. T. R. Fukuda, J. Hasegawa, M. Ishida, T. Nakajima, Y. Honda, O. K. H. Nakai, T. Vreven, J. A. Montgomery, Jr, J. E. Peralta, F. O. M. Bearpark, J. J. Heyd, E. Brothers, K. N. Kudin, V. N. Staroverov, R. Kobayashi, J. Normand, K. Raghavachari, A. Rendell, J. C. Burant, S. S. Iyengar, J. Tomasi, M. Cossi, N. R. J. M. Millam, M. Klene, J. E. Knox, J. B. Cross, V. Bakken, C. A. J. Jaramillo, R. Gomperts, R. E. Stratmann, O. Yazyev, A. J. Austin, R. Cammi, C. Pomelli, J. W. Ochterski, R. L. Martin, K. Morokuma, V. G. Zakrzewski, G. A. Voth, P. Salvador, J. J. Dannenberg, S. Dapprich, A. D. Daniels, O. Farkas, J. B. Foresman, J. V. Ortiz, J. Cioslowski and D. J. Fox (2009). Gaussian, Inc, Wallingford, CT.

(29) R. Dennington, T. Keith, J. Millam. (2009) GaussView 5. Semichem Inc, Shawnee Mission KS.

(30) Jensen, F. (2007) Introduction to Computational Chemistry, 2nd edn. Wiley, Chichester, UK.

(31) CambridgeSoft Corporation. (2013) ChemBio3D Ultra 13.0. CambridgeSoft Corporation, Cambridge, UK.

(32) Bousquet, D., R. Fukuda, D. Jacquemin, I. Ciofini, C. Adamo and M. Ehara (2014) Benchmark Study on the Triplet Excited-State Geometries and Phosphorescence Energies of Heterocyclic Compounds: Comparison Between TD-PBE0 and SAC-CI. *J. Chem. Theory Comput.* **10**, 3969−3979.

(33) Norberg, D., P. Larsson and N. Salhi-Benachenhou (2008) Rearrangement and Hydrogen Scrambling Pathways of the Toluene Radical Cation: A Computational Study. *J. Phys. Chem. A.* **112**, 4694–4702.

(34) Bulo, R. E., H. Jansen, A. W. Ehlers, F. J. J. de Kanter, Fransiscus, M. Schakel, M. Lutz, A. L. Spek and K. Lammerisma (2004) The Circumambulation of a Phosphirane: Taking 9-Phenyl-9-phosphabicyclo[6.1.0]nona-2,4,6-triene for a "Walk". *Angew. Chem. Int. Ed.* **43**, 714–717.

(35) Gruetzmacher, H. and N. Harting (2003) A Ring Walk of Methylene Groups in Toluene Radical Cations. An Extension of the Toluene-cycloheptatriene Rearrangement of Aromatic Radical Cations. Theory and Experiment. *Eur. J. Mass Spectrom.* **9**, 327–341.

(36) Alder, R. W., S. P. East, J. N. Harvey and M. T. Oakley (2003) The Azulene-to-Naphthalene Rearrangement Revisited: a DFT Study of Intramolecular and Radical-Promoted Mechanisms. *J. Am. Chem. Soc.* **125**, 5375–5387.

(37) Klärner, F. G., V. Glock and J. L. Hemmes (1990) Mechanism of the Cyclopropane "Walk" Rearrangement: Syntheses and Properties of 2-Diazopropane-arene Adducts; a Regiospecific Nitrogen Elimination. *Ber. Dtsch. Chem. Ges.* **123**, 1869–1879.

(38) Zimmerman, H. E. and S. M. Aasen (1973) Mechanistic and Exploratory Organic Photochemistry. 107. Vinylcyclopropene Photochemistry: Photochemistry Applied to Organic Synthesis. Exploratory and Mechanistic Organic Photochemistry. *J. Org. Chem.* **43**, 1493–1506.

(39) Zimmerman, H. E. and W. Eberbach (1973) Walk Rearrangement of a Diazanorcaradiene. Mechanistic and Exploratory Organic Photochemistry. LXXVIII. *J. Am. Chem. Soc.* **95**, 3970–3976.

(40) Zimmerman, H. E., D. F. Juers, J. M. McCall and B. Schroeder (1970) Walk Processes in Photochemical Molecular Rearrangements. General Photochemical Transformation. Mechanistic and Exploratory Organic Photochemistry. LVII. *J. Am. Chem. Soc.* **92**, 3474–3476.

(41) Shanoski, J. E., E. A. Glascoe and C. B. Harris (2006) Ligand Rearrangement Reactions of $Cr(CO)_6$ in Alcohol Solutions: Experiment and Theory. *J. Phys. Chem. B* **110**, 996–1005.

(42) Kislov, V. V. and A. M. Mebel (2007) The Formation of Naphthalene, Azulene, and Fulvalene from Cyclic C5 Species in Combustion: an Ab Initio/RRKM Study of 9-*H*-fulvalenyl (C_5H_5-C_5H_4) Radical Rearrangements. *J. Phys. Chem. A* **111**, 9532–9543.

(43) Sena, M. and J. M. Riveros (2000) Ring-hydrogen Participation in the Keto-enol Isomerization of the Acetophenone Radical Cation. *Chem. Eur. J.* **6**, 785–793.

(44) Jensen, F. (1989) The Walk Rearrangement in Bicyclo[2.1.0]pent-2-ene. An MCSCF Study. *J. Am. Chem. Soc.* **111**, 4643–4647.

(45) Wainwright, M., R. M. Giddens (2003) Phenothiazinium Photosensitisers: Choices in Synthesis and Application. *Dyes Pigm.* **57**, 245–257.

(46) Groehn, V., L. Fröhlich, H. Schmidt, and W. Pfleiderer (2000) Pteridines, Part CXI, Pteridine‐Based Photoaffinity Probes for Nitric Oxide Synthase and Aromatic Amino Acid Hydroxylases. *Helv. Chim. Acta* **83**, 2738–2750.

(47) Phillips, D. (2011) IUPAC Commission, Toward Targeted Photodynamic Therapy. *Pure Appl. Chem.* **83**, 733–748.

(48) Lee, H. Y., J. H. Kim, J. S. Yoo, J. H. Bae, C. Yoon and J. H. Choi (2014) Synthesis and Thermal Stability of Solvent Soluble Dyes Based on Dimerized Diketo-pyrrolo-pyrrole Pigment. *Bull. Korean Chem. Soc.* **35**, 659–662.

(49) Waser, M. and H. Falk (2011) Progress in the Chemistry of Second Generation Hypericin Based Photosensitizers. *Curr. Org. Chem.* **15**, 3894–3907.

(50) Chen, X., X. Xu and Z. Cao (2007) Theoretical Study on Singlet Excited State of Pterin and Its Deactivation Pathway. *J. Phys. Chem. A* **111**, 9255–9262.

(51) Ji, H.-F., and L. Shen (2011) Mechanistic Study of ROS Photogeneration by Pterin. *Pteridines* **22**, 73–76.

(52) Baptista, M. S., J. Cadet, P. Di Mascio, A. A. Ghogare, A. Greer, M. R. Hamblin, C. Lorente, S. C. Nunez, M. S. Ribeiro, A. H. Thomas, M. V. Vignoni and T. M. Yoshimura. Type I and II Photosensitized Oxidation Reactions: Guidelines and Mechanistic Pathways. *Photochem. Photobiol.* **93**, 912–919.

(53) Ghogare, A. A. and A. Greer (2016) Using Singlet Oxygen to Synthesize Natural Products and Drugs. *Chem. Rev.* **116**, 9994–10034.

(54) Reibnegger, G. (2015) An *ab initio* and Density Functional Theory Study on Neutral Pterin Radicals. *Pteridines* **26**, 135–142.

(55) Martin, C. B., D. Walker and M. Soniat (2009) Density Functional Theory Study of Possible Mechanisms of Folic Acid Photodecomposition. *J. Photochem. Photobiol. A* **208**, 1–6.

(56) DiScipio, R. M., R. Y. Santiago, D. Taylor and C. E. Crespo-Hernandez (2017) Electronic Relaxation Pathways of the Biologically Relevant Pterin Chromophore. *Phys. Chem. Chem. Phys.* **19**, 12720–12729.

(57) Heyne, B. Self-assembly of Organic Dynes in Supramolecular Aggregates. *Photochem. Photochem. Sci.* **15**, 1103–1114.

(58) Liu, J., J. Li, Z. Zhang, Y. Weng, G. Chen, B. Yuan, K. Yang and Y. Ma (2014) Encapsulation of Hydrophobic Phthalocyanine with Poly(*N*-isopropylacrylamide)/lipid Composite Microspheres for Thermo-responsive Release and Photodynamic Therapy. *Materials* **7**, 3481–3493.

(59) Mallory, F. B., C. W. Mallory, C. K. Regan, R. J. Aspden, A. B. Ricks, J. M. Racowski, A. I. Nash, A. V. Gibbions, P. J. Carroll and J. M. Bohen (2013) Phenyl Groups versus *tert*-Butyl Groups as Solubilizing Substituents for Some [5]Phenacenes and [7]Phenacenes. *J. Org. Chem.* **78**, 2040–2045.

(60) Hallett, A. J., N. White, W. Wu, X. Cui, P. N. Horton, S. J. Coles, J. Zhao and S. J. A. Pope (2012) Enhanced Photooxidation Sensitizers: The First Examples of Cyclometalated Pyrene Complexes of Iridium(III). *Chem. Comm.* **48**, 10838–10840.

(61) Ol'shevskaya, V. A., R. G. Nikitina, A. N. Savchenko, M. V. Malshakova, A. M. Vinogradov, G. V. Golovina, D. V. Belykh, A. V. Kutchin, M. A. Kaplan, V. N. Kalinin, V. A. Kuzmin and A. A. Shtil (2009) Novel Boronated Chlorin e_6-based Photosensitizers: Synthesis, Binding to Albumin and Antitumor Efficacy. *Bioorganic Med. Chem.* **17**, 1297–1306.

(62) Pu, H. and G. Liu (2005) Synthesis and Solubility of Poly(*N*-methylbenzimidazole) and Poly(*N*-ethylbenzimidazole): Control of Degree of Alkylation. *Polym. Int.* **54**, 175–179.

(63) Mori, T., M. Takamoto, Y. Tate, J. Shinkuma, T. Wada and Y. Inoue (2001) Photoinduced Electron Transfer Oxidation of α-Methylstyrene with Molecular Oxygen Sensitized by Dimethoxybenzenes: a Non-singlet-oxygen Mechanism. *Tetrahedron Lett.* **42**, 2505–2508.

(64) Makareeva, E. N., E. L. Lozovskaya and I. I. Sapezhinskii (1998) Phenothiazine Drugs as Photosensitizers and Photoprotectors. *Biofizika* **43**, 181–185.

(65) Pandey, R. K., A. B. Sumlin, S. Constantine, M. Aoudla, W. R. Potter, D. A. Bellnier, B. W. Henderson, M. A. Rodgers, K. M. Smith and T. J. Dougherty (1996) Alkyl Ether Analogs of Chlorophyll-a Derivatives: Part 1. Synthesis, Photophysical Properties and Photodynamic Efficacy. *Photochem. Photobiol.* **64**, 194–204.

(66) Martinez-Haya, R., M. A. Miranda and M. L. Marin (2017) Type I vs Type II Photodegradation of Pollutants. *Catal. Today*, Ahead of Print.

(67) Macia, N., B. Heyne (2015) Using Photochemistry to Understand and Control the Production of Reactive Oxygen Species in Biological Environments. *J. Photochem. Photobiol. A* **306**, 1–12.

(68) Petroselli, G., M. L. Dántola, F. M. Cabrerizo, A. L. Capparelli, C. Lorente, E. Oliveros and A. H. Thomas (2008) Oxidation of 2'-Deoxyguanosine 5'-Monophosphate Photoinduced by Pterin: Type I Versus Type II Mechanism. *J. Am. Chem. Soc.* **130**, 3001–3011.

FIGURE CAPTIONS

Figure 1. Parent pterin **1**, alkylated pterins **2**-**4**, an alkylated porphyrin **5**, and a TBDMS-substituted guanosine **6**. Atom numbering will not use subscripts to denote exocyclic atoms.

Figure 2. Synthesis reaction for pterins **3** and **4**.

Figure 3. (a) The expanded 2D HMBC spectrum of pterins **3** in DMSO-d_6 shows a $^3J_{CH}$ correlation (X) between O−CH_2 protons coupled to carbon b suggesting O^4-alkylation (b) The expanded 2D HMBC spectrum of pterin **4** in DMSO-d_6 shows two $^3J_{CH}$ correlations (Y,Z) between the N−CH_2 protons coupled to carbons a′ and b′ suggesting N3 alkylation.

Figure 4. Schematic of the possible role of a walk rearrangement of the R group around the pterin periphery.

Figure 5. Possible mechanisms of alkyl pterin rearrangement: (a) concerted alkyl ”walk” rearrangement, (b) a dissociative pathway through ions, and (c) a dissociative pathway through radical pair formation. The B3LYP/D95** optimized structures are shown for **2b** and **2**.

Figure 6. B3LYP/D95** potential energy surface of minimum energy structures and transition states (TS) for **2b** and **2** (R = methyl) (A), and **2b** anion and **2** anion (R = methyl) (B), and minimum energy structures for **3** and **4** (R = decyl). Further calculations on **2b** and **2** show that the formation of a radical pair, or ion pair intermediate both require >60 kcal/mol energy. Relative enthalpies in kcal/mol.

Figure 7. B3LYP/D95** computed potential energy surface (PES) for a walk rearrangement of the methyl group around the periphery of the pterin ring in a counter clockwise direction. Compounds **2′**, **2**, and **2b**–**2i** optimized to minima, where species labeled “TS” are saddle points.

Figure 8. DFT computed molecular orbitals for the parent and alkylated pterins, in which the positive isovalues are in red, and the negative isovalues are in green. Isovalue = 0.01.

Figure 9. HPLC chromatogram recorded at 360 nm of a methanol/water (50/50) solution of pterin **3** (75 μM, retention time = 13.8 min) prior to (black line) and after (red line) UVA irradiation for 120 min. Inset: time-evolution of pterin **3** concentration upon UVA irradiation.

TABLE CAPTIONS

Table 1. ^{1}H and ^{13}C NMR data for pterins **3** and **4**.

Table 2. 2D HSQC correlations of ^{1}H protons with ^{13}C.

Table 3. 2D HMBC correlations of ^{1}H protons with aromatic ^{13}C.

Table 4. Synthesized percent yields of pterins **3** and **4** under different reaction conditions.

Table 5. Effect of alkylation on pterin on the log *P* and log *D* values.

Table 6. Computed and experimental information on the parent and alkylated pterins.

Table 7. TD-DFT computed electronic excitation properties for the parent and alkylated pterins.

Table 1. ^{13}C and ^{1}H NMR data for pterins **3** and **4**.

position	pterin **3**		position	pterin **4**	
	^{13}C signal/ δ (ppm)	^{1}H signal/ δ (ppm)		^{13}C signal/ δ (ppm)	^{1}H signal/ δ (ppm)
b	166.9		b'	160.7	
a	161.6		f’	155.8	
f	157.2		a’	153.9	
d	150.9	8.78	d’	150.0	8.66
c	139.5	8.43	c’	139.1	8.36
e	123.4		e’	128.0	
O4-CH_2	67.2	4.46	N3-CH_2	41.7	3.95

Table 2. 2D HSQC correlations of ^{1}H protons with ^{13}C.

pterin **3**		pterin **4**	
^{13}C signal/ δ (ppm)	HSQC cross signal	^{13}C signal/ δ (ppm)	HSQC cross signal
166.9	-	160.7	-
161.6	-	155.8	-
157.2	-	153.9	-
150.9	8.78	150.0	8.66
139.5	8.43	139.1	8.36
123.4	-	128.0	-
67.2	4.46	41.7	3.95

Table 3. 2D HMBC correlations of ^{1}H protons with aromatic ^{13}C.

pterin **3**		pterin **4**	
^{1}H signal/ δ (ppm)	^{13}C correlated peaks/ δ (ppm)	^{13}C signal/ δ (ppm)	^{13}C correlated peaks/ δ (ppm)
8.78	139.5, 157.2	8.66	139.1, 155.8
8.43	123.4, 150.9	8.36	128.0, 150.0
4.46	166.9	3.95	152.9, 160.7

Table 4. Synthesized percent yields of pterins **3** and **4** under different reaction conditions.

entry	solvent	temperature (°C)	base	yields of products (%)	
				3	**4**
1	DMF	25-40	K_2CO_3	0	0
2	DMF	60	K_2CO_3	35 [a]	25 [a]
3	DMF	70	K_2CO_3	37 [a]	20 [a]
4	DMF	90	K_2CO_3	0	0
5	DMF	70	NaOH	0	0
6	DMA	70	K_2CO_3	40 [a]	25 [a]
7	THF	70	K_2CO_3	~6 [b]	~3 [b]
8	DCM	40	K_2CO_3	0	0

[a] Isolated yields.

[b] Detected in the reaction mixture by ^{1}H MMR spectroscopy.

Table 5. Computed solubilities of pterin derivatives.

pterin	computed lo□ P^a	computed lo□ D^a			reference
		pH = 3	pH = 7	pH = 11	
1		-0.96	–0.16	–1.96	this work
2	-0.□9	-0.□9	-0.□9	-0.□9	this work
3	3.53	3.52	3.53	3.53	□
4	2.81	2.81	2.81	2.81	□

[a]Computed with the MarvinSketch 17.1.2(ChemAxon Ltd. Budapest, Hungary).

Table 6. Computed and experimental information on the parent and alkylated pterins.

Compound	Computed		Experimental				
	S_0 - S_1 kcal/mol	S_0 - T_1 kcal/mol	S_0 - S_1 kcal/mol	S_0 - T_1 kcal/mol	fluorescence quantum yield Φ_F ± SD	$^1O_2$ quantum yield Φ_Δ ± SD	Ref.
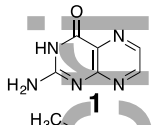 **1**	81.3	68.0	71.4	58.1	0.33 ± 0.02	0.18 ± 0.02	5,8
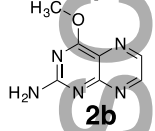 **2b**	75.4	64.4	—	—	—	—	8
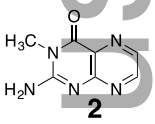 **2**	80.8	67.6	—	—	—	—	8
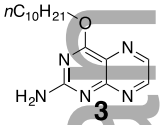 **3**	76.0	64.3	—	—	0.012 ± 0.002	0.50 ± 0.02	8
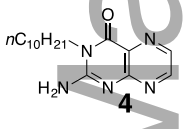 **4**	80.6	67.6	—	—	0.078 ± 0.008	0.37 ± 0.02	8

Table 7. TD-DFT computed electronic excitation properties for the parent and alkylated pterins.

Compound	Transition	Major contributions	Assignment
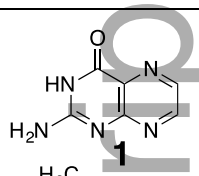 **1**	S_0 - T_1	HOMO-1 ⟶ LUMO (91%)	n ⟶ π*
	S_0 - S_1	HOMO-1 ⟶ LUMO (98%)	n ⟶ π*
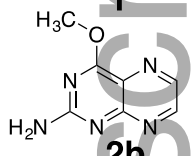 **2b**	S_0 - T_1	HOMO ⟶ LUMO (95%)	π ⟶ π*
	S_0 - S_1	HOMO-1 ⟶ LUMO (99%)	n ⟶ π*
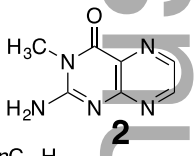 **2**	S_0 - T_1	HOMO-1 ⟶ LUMO (89%)	n ⟶ π*
	S_0 - S_1	HOMO-1 ⟶ LUMO (99%)	n ⟶ π*
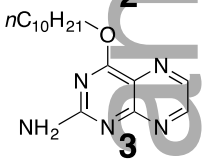 **3**	S_0 - T_1	HOMO ⟶ LUMO (95%)	π ⟶ π*
	S_0 - S_1	HOMO-1 ⟶ LUMO (99%)	n ⟶ π*
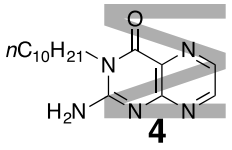 **4**	S_0 - T_1	HOMO-1 ⟶ LUMO (87%)	n ⟶ π*
	S_0 - S_1	HOMO-1 ⟶ LUMO (99%)	n ⟶ π*

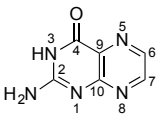

1

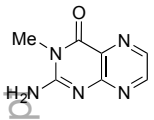

2

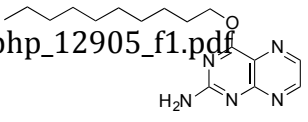

3

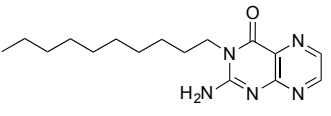

4

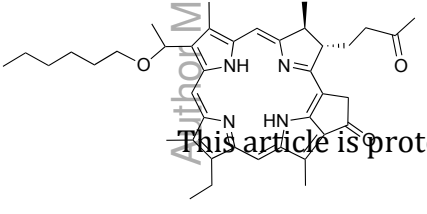

5

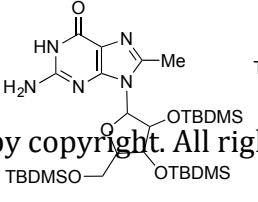

6

TBDMS = *tert*-butyldumethylsilyl

1 3 4

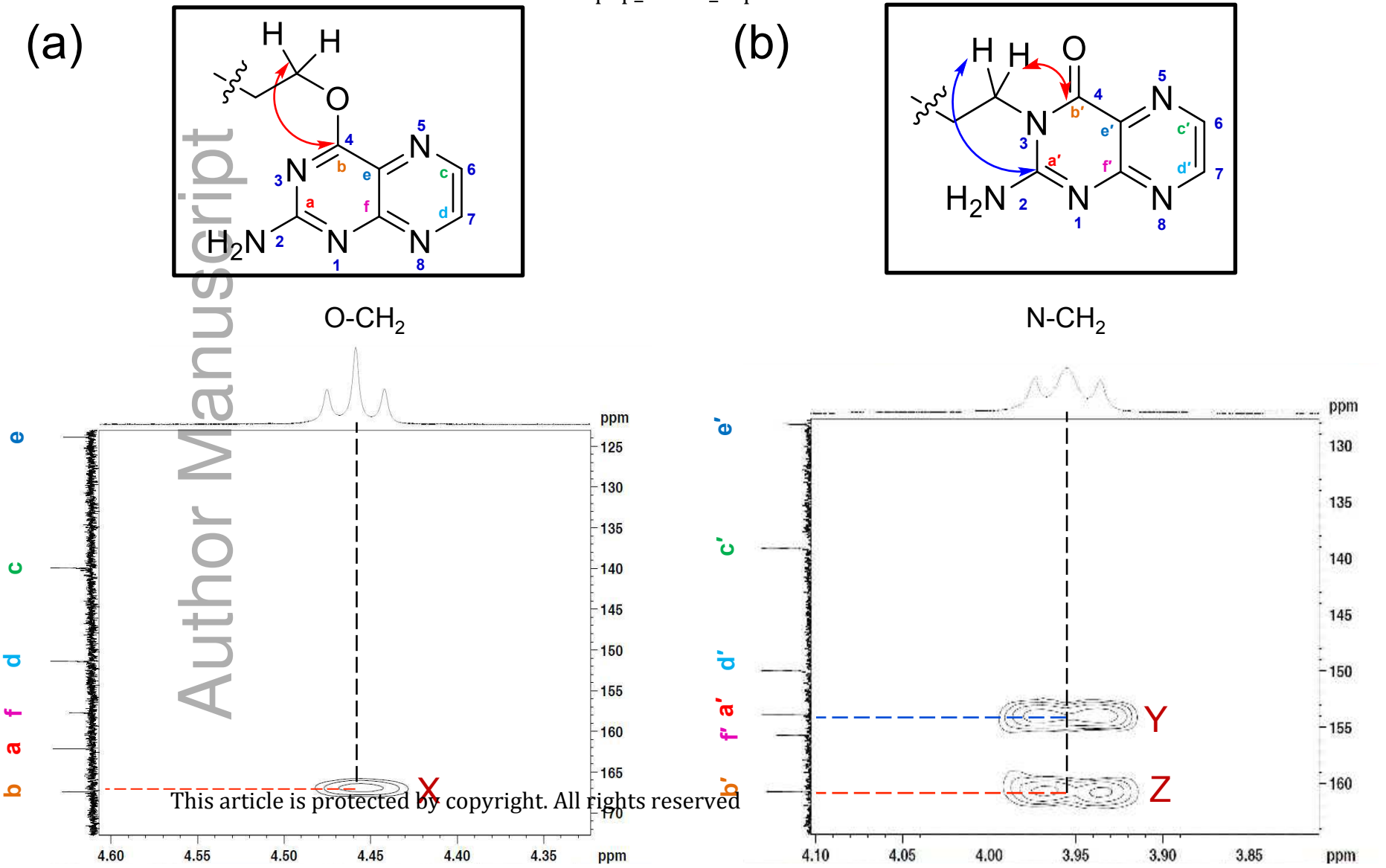

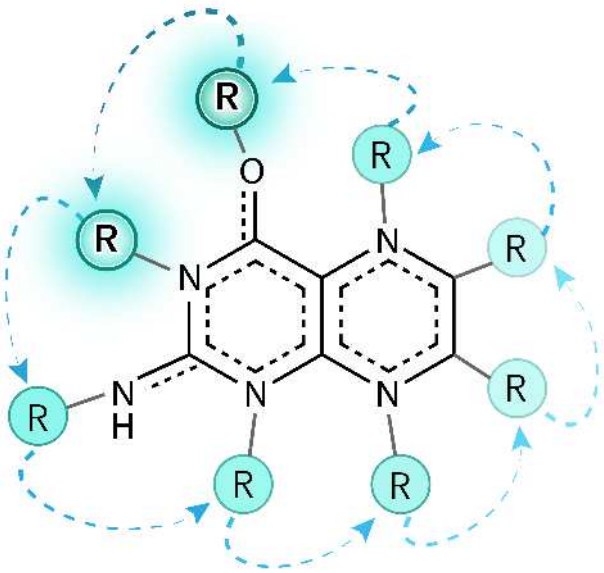

php_12905_f4.jpg

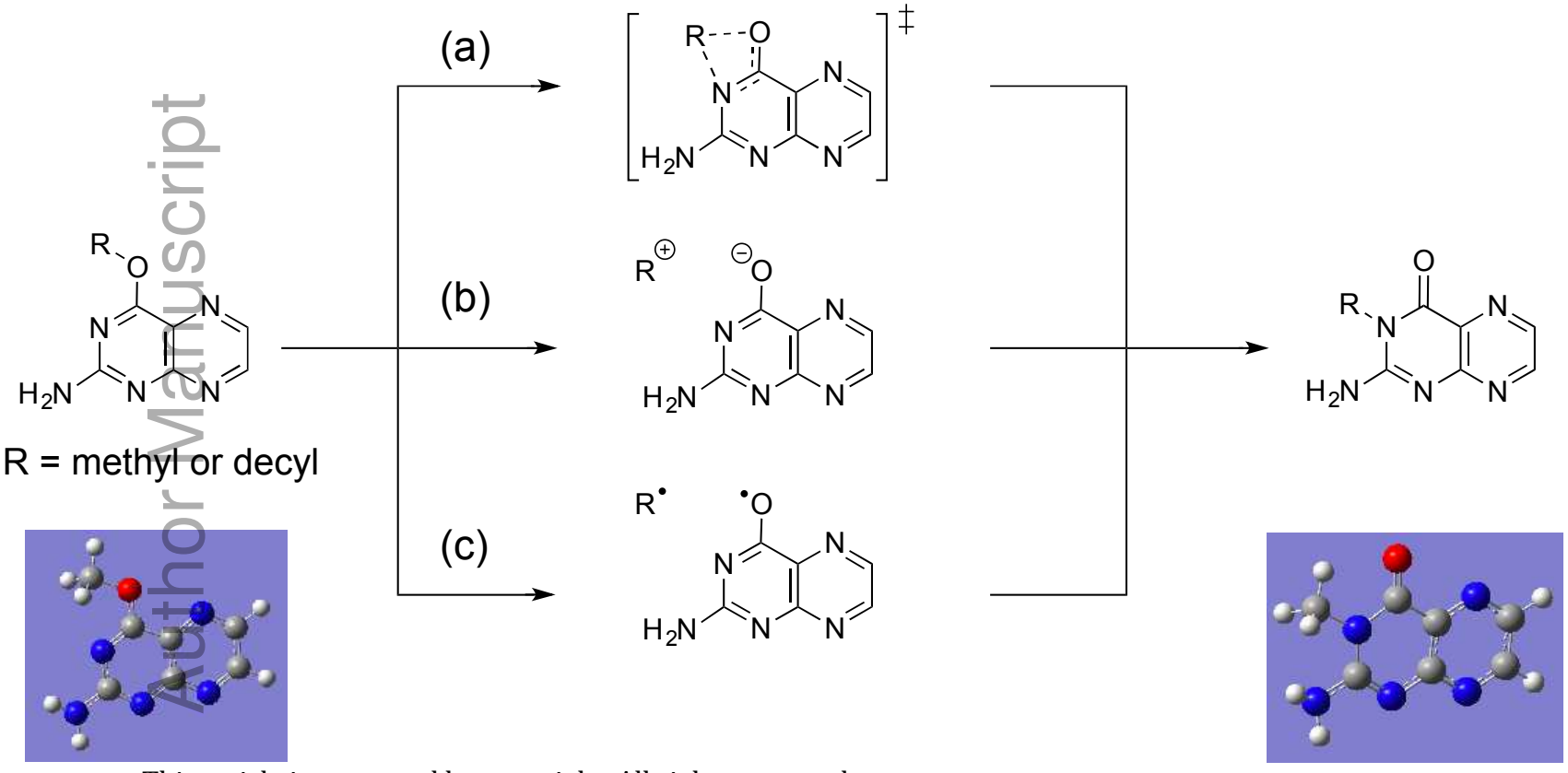

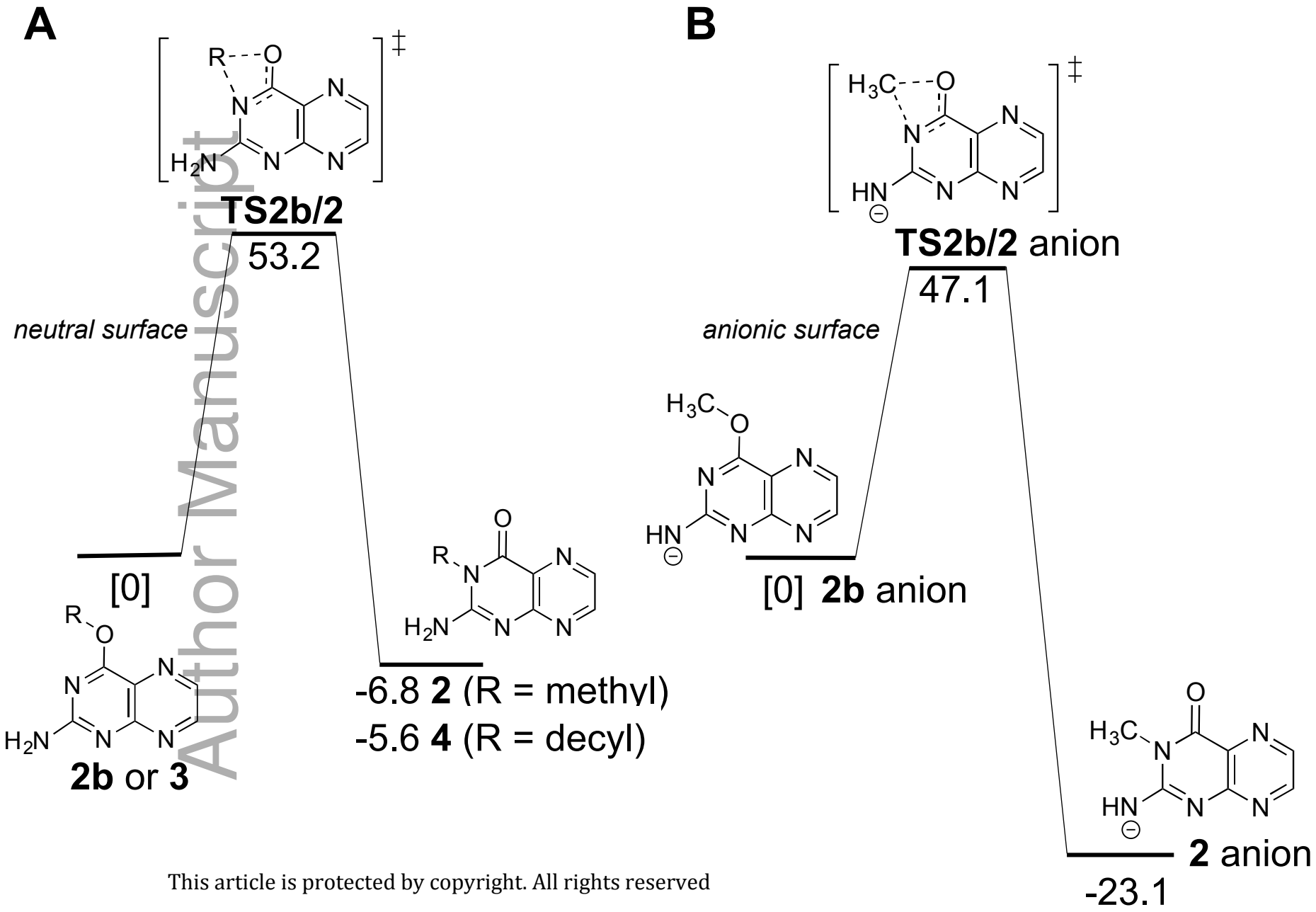

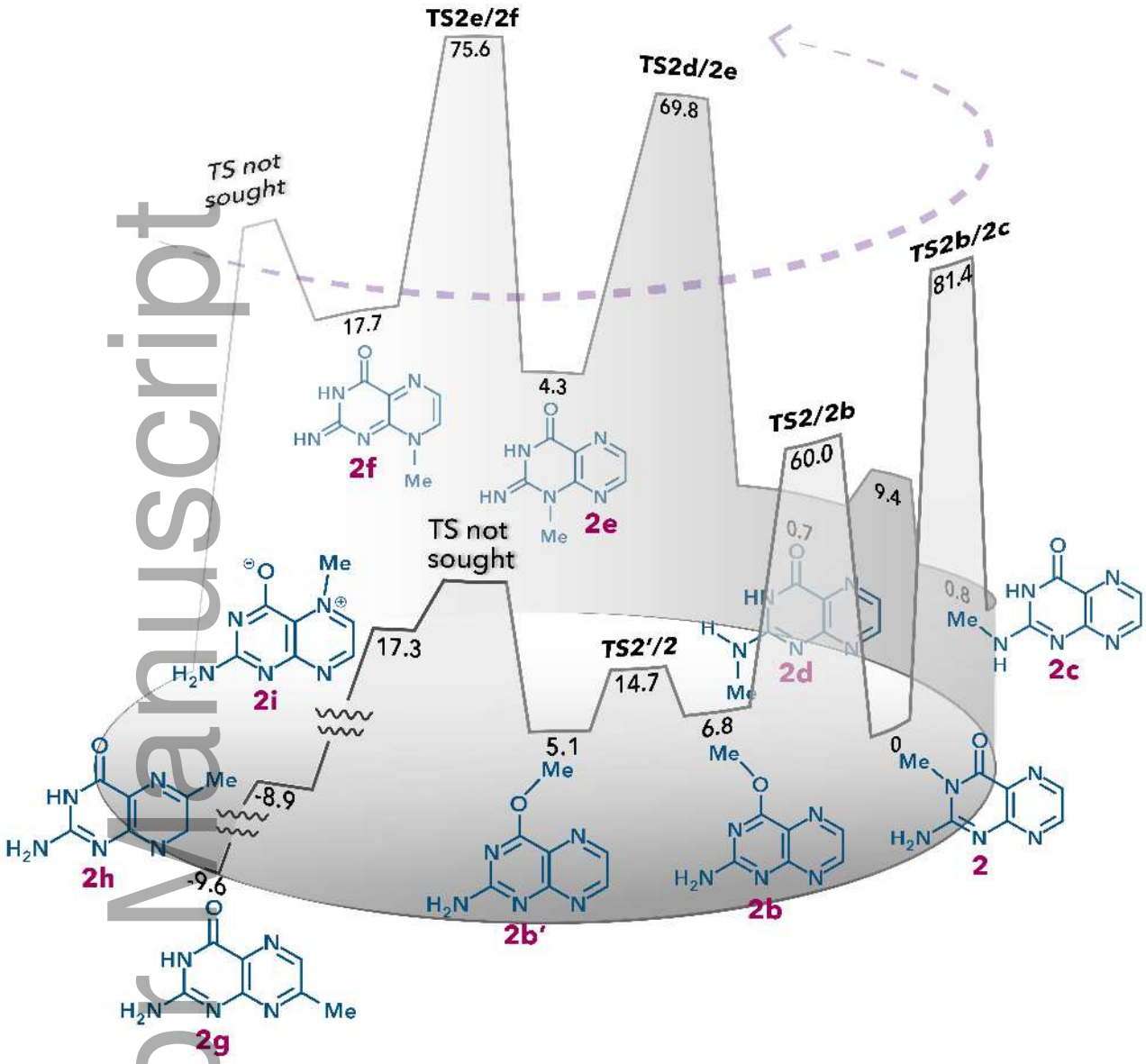

php_12905_f7.jpg

Compound	HOMO-1	HOMO	LUMO
1	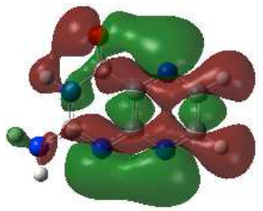	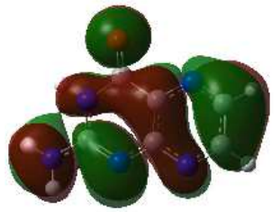	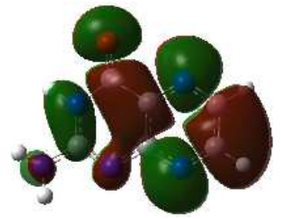
2b	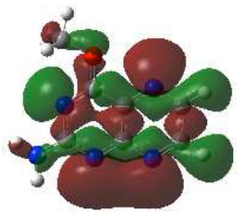	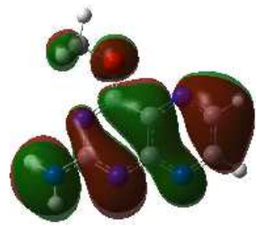	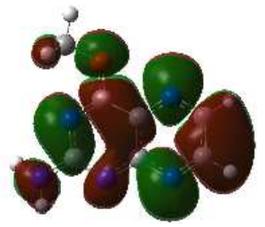
2	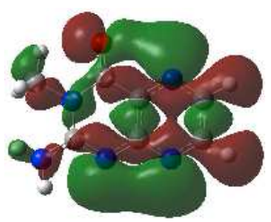	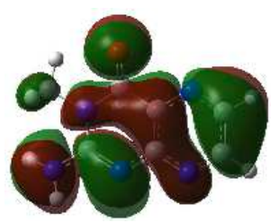	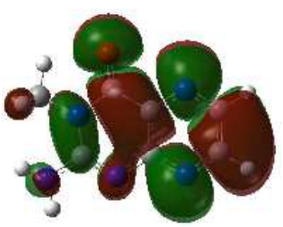
3	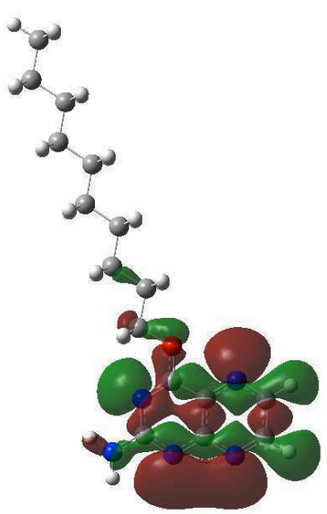	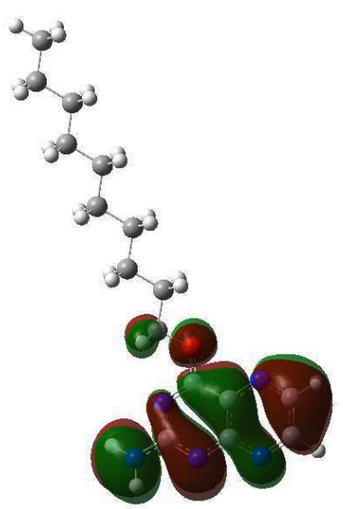	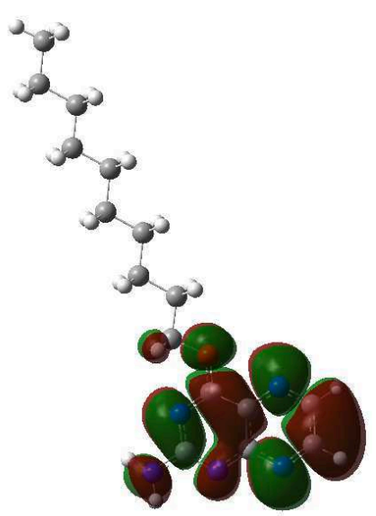
4